Digital Signal Processing 69 (2017) 309–322

Contents lists available at ScienceDirect

Digital Signal Processing

www.elsevier.com/locate/dsp

A novel approach for time–frequency localization of scaling functions and design of three-band biorthogonal linear phase wavelet filter banks

Dinesh Bhati [a,*], Ram Bilas Pachori [b], Vikram M. Gadre [a]

[a] Department of Electrical Engineering, Indian Institute of Technology, Bombay, Mumbai, India
[b] Discipline of Electrical Engineering, Indian Institute of Technology Indore, Indore, India

ARTICLE INFO

Article history:
Available online 13 July 2017

Keywords:
Time-frequency localization
Three-band wavelet filter bank
Discrete Fourier transform
Discrete time Fourier transform
Prolate spheroid sequence

ABSTRACT

Design of time–frequency localized filters and functions is a classical subject in the field of signal processing. Gabor's uncertainty principle states that a function cannot be localized in time and frequency domain simultaneously and there exists a nonzero lower bound of 0.25 on the product of its time variance and frequency variance called time–frequency product (TFP). Using arithmetic mean (AM)–geometric mean (GM) inequality, product of variances and sum of variances can be related and it can be shown that sum of variances has lower bound of one. In this paper, we compute the frequency variance of the filter from its discrete Fourier transform (DFT) and propose an equivalent summation based discrete-time uncertainty principle which has the lower bound of one. We evaluate the performance of the proposed discrete-time time–frequency uncertainty measure in multiresolution setting and show that the proposed DFT based concentration measure generate sequences which are even more localized in time and frequency domain than that obtained from the Slepian, Ishii and Furukawa's concentration measures. The proposed design approach provides the flexibility in which the TFP can be made arbitrarily close to the lowest possible lower bound of 0.25 by increasing the length of the filter. In the other proposed approach, the sum of the time variance and frequency variance is used to formulate a positive definite matrix to measure the time–frequency joint localization of a bandlimited function from its samples. We design the time–frequency localized bandlimited low pass scaling and band pass wavelet functions using the eigenvectors of the formulated positive definite matrix. The samples of the time–frequency localized bandlimited function are obtained from the eigenvector of the positive definite matrix corresponding to its minimum eigenvalue. The TFP of the designed bandlimited scaling and wavelet functions are close to the lowest possible lower bound of 0.25 and 2.25 respectively. We propose a design method for time–frequency localized three-band biorthogonal linear phase (BOLP) wavelet perfect reconstruction filter bank (PRFB) wherein the free parameters can be optimized for time–frequency localization of the synthesis basis functions for the specified frequency variance of the analysis scaling function. The performance of the designed filter bank is evaluated in classification of seizure and seizure-free electroencephalogram (EEG) signals. It is found that the proposed filter bank outperforms other existing methods for the classification of seizure and seizure-free EEG signals.

1. Introduction

In the last two decades, wavelet filter banks have played a key role in describing nonstationary signals such as speech, seismic, radar, electroencephalogram (EEG), electrocardiogram (ECG) [1–3]. The basis functions generated by the wavelet filter bank provide multiple resolutions in time domain and frequency domain. Time–frequency localized wavelet bases are desirable in signal analysis [4–6], image coding [7–9,8,10], edge detection and image segmentation [11,12]. The joint time–frequency localization of the wavelet basis functions is generally represented by the dimensions of the tile on the time–frequency plane [13] that represents them. The area of the tile or the time–frequency product (TFP) represents the joint localization of the basis function in the time and frequency domain. Various signal processing applications require trade-off in time localization and frequency localization. For example, time localized bases preserve the edges in the image whereas bandwidth

* Corresponding author.
E-mail addresses: bhatidinesh@gmail.com (D. Bhati), pachori@iiti.ac.in (R.B. Pachori), vmgadre@ee.iitb.ac.in (V.M. Gadre).

http://dx.doi.org/10.1016/j.dsp.2017.07.008
1051-2004/

compression of an image can be achieved with good frequency localization. In this paper, we propose a novel design method for time–frequency localization of a regular scaling filter and the corresponding scaling function. We show that the proposed method outperforms Slepians' [14], Ishii and Furukawas' [15] methods for time–frequency localization of discrete scaling filters as well as continuous scaling functions. We use the concentration measures for time-limited functions proposed by Bhati et al. [16] and propose a design method for the time–frequency localized three-band biorthogonal linear phase (BOLP) wavelet filter bank of length nine and regularity order of one. The design problem of time–frequency localized wavelet filter banks can be addressed in two different ways, that directly affects the complexity of the design problem. Time–frequency localized wavelet filter banks can be designed either by time–frequency localization of scaling and wavelet functions [17–19,16], or the filters of a regular perfect reconstruction filter bank (PRFB) [8,20–23]. The former deals with Heisenberg uncertainty principle (HUP) for signals in $L_2(\mathbb{R})$ and the later is based on HUP for signals in $L_2(\mathbb{Z})$. The time–frequency localized filters do not ensure that the corresponding scaling and wavelet functions are also well localized in time and frequency domain. Therefore, in this paper, we propose a design method in which we use the expressions for time variance and frequency variance proposed by Bhati et al. [16] and the sum of the weighted TFPs of the scaling and wavelet functions is minimized with respect to the free parameters of the filter bank.

There are various notions in the literature to measure the effective support of a function in time or frequency domain [24,14,5,15,25]. Slepian et al. [14] measures the energy concentration in the given frequency band for time-limited signals whereas, Gabor uses the notion of variances to measure the effective supports in time and frequency domains [5]. Time–frequency uncertainty principle (UP) in discrete domain is studied by several authors in the literature. Ishii and Furukawa [15] proposed time–frequency UP for discrete time sequences. Gabor showed that signals in $L_2(\Re)$ cannot be localized simultaneously in time and frequency domain and there exists a lower bound of 0.25 on the TFP [5]. Chui et al. [26] determine the similar uncertainty lower bound for band pass functions. Venkatesh et al. [25] studied the limitations of UP proposed by Ishii and Furukawa [15]. They obtained the continuous time signal from the samples of the symmetric low pass bandlimited signal by interpolation and removed the inconsistency between the definitions of discrete-time and continuous-time variances. However, the variance expressions proposed by them are applicable to zero phase low pass bandlimited functions only.

Nam [27] formulates the discrete-time measure to quantify the uncertainty in time–frequency analysis using the discrete Fourier transform (DFT) for a subclass of finite length discrete signals. They derive the relation between the uncertainties for discrete-time and continuous-time cases. However, they do not determine the filter or the function optimally localized in time and frequency domains. Parhizkar et al. [28] design the time–frequency localized filter however, the filter is not a regular scaling filter and do not generate a time–frequency localized scaling function. Lebedeva and Prestin [29] used the notion of Brietenberg uncertainty constant and proposed the Parseval periodic wavelet frames optimally localized in time and frequency domain. However, they do not determine the corresponding time–frequency localized discrete-time regular scaling filter. Sharma et al. [20] reduced the design complexity associated with the product of variances and proposed minimization of sum of variances to design time–frequency localized wavelet filter banks. They design the time–frequency localized filter using eigenfilter approach. However, in order to simplify the design problem, they impose the unit norm constraint on the half of the filter coefficients of the linear phase filter and therefore the designed eigenfilters are not optimally localized in time and frequency domain. Sharma et al. [30] design time–frequency localized scaling filter for the specified time variance or frequency variance of the filter. Sharma et al. [31] use UP for linear operators to design time–frequency localized filter, however, they do not impose the regularity constraint to obtain the time–frequency localized scaling filter and function. Bhati et al. [16] design the time–frequency localized scaling function as well as scaling filter, however, the designed scaling filter is not optimally localized with TFP close to 0.25. Gabor's UP [5] for continuous-time functions is generally studied assuming function $f(t) \in L_2(\Re)$ [32,33,25,34]. Bhati et al. [16] emphasize that $tf(t) \in L_2(\Re)$ and $\frac{df(t)}{dt} \in L_2(\Re)$ together imply $f(t) \in L_2(\Re)$. Bhati et al. [35] design time–frequency localized regular linear phase scaling filters, optimally localized in time and frequency domains, however, the proposed semidefinite relaxation does not ensure time–frequency localization of scaling function generated from the cascade iterations of the designed scaling filter.

In this paper, the notions of prolate spheroid wave functions (PSWF) and the HUP are used to design the time–frequency localized scaling filter which generates the time–frequency localized scaling function with TFP close to the lowest possible lower bound of 0.25. In the approach based on PSWF, we maximize the energy of the time-limited filter in a specified bandwidth and propose a design method which ensures time–frequency localization of scaling filter as well as the scaling function. Bhati et al. [16] design time–frequency localized scaling function with unit Sobolev regularity. In this work, we use a scaling filter with regularity order of two and design a time–frequency localized scaling function with Sobolev regularity of two. HUP for linear operators is used in the second approach subject to the linear constraints for regularity to design time–frequency localized scaling filter and the function. Sharma et al. [31] use the notion of quantum harmonic oscillator and DFT and propose the discrete-time UP which is an equivalent of Gabor's UP for continuous time functions. In this paper, we compute the frequency variance of filter from its DFT and propose a much simpler approach as compared to the method proposed by Sharma et al. [31]. We compare the performance of proposed UP with that proposed by Slepian [14] and Ishii and Furukawa [15] employing the discrete time Fourier transform (DTFT) of the filter to measure its frequency variance. In another proposed approach in the paper, the sum of time variance and frequency variance is used to formulate a positive definite matrix and the eigenvectors of the proposed positive definite matrix are used to obtain the samples of time–frequency localized bandlimited scaling and wavelet functions. In the proposed method, we modify the product form of discrete-time uncertainty measure proposed by Venkatesh et al. [25] to the summation form and use it to design the bandlimited low pass function with TFP close to the lowest possible lower bound of 0.25. This method simplifies the condition of regularity of the scaling function, therefore, we further use it for the design of time–frequency localized three-band filter bank.

The spectral characteristics of the basis functions greatly affect the performance of the filter bank in signal classification [36]. Two-band ideal filter banks suffer from poor frequency resolution in the low as well as high frequency band with frequency resolution of each band equal to $\Delta\omega = \pi/2$ [37,35]. Two-band wavelet filter banks generate the wavelet basis functions from its successive cascade iterations on the low pass filter branch. Provided the conditions for regularity of the filters are satisfied, each successive cascade iteration on the low pass branch generates smooth wavelet basis functions to analyze the signals in their low frequency bands. Though the low pass and band pass basis functions of the commonly used wavelet filter bank are localized in time and frequency domains, the cascade iterative structure used in wavelet multiresolution analysis suffers from the drawback that successive basis functions analyze the low frequency band only and not the high frequency components of the sig-

nal. Higher number of cascade iterations can be used to analyze the signals with very high frequency resolution in the low frequency band. It should be noted that the successive cascade iterations of the two-band wavelet transform do not improve the frequency resolution of the basis functions in the high frequency band. Furthermore, the successive cascade iterations increase the attenuation of the magnitude spectrum of the iterated filters in the high frequency band. Thus, two-band wavelet filter banks suffer from poor analysis of signals having significant energy in the high frequency band. The ideal M-band filter bank with $M > 2$ subbands is the extension of the two-band filter bank, which improves the subband frequency resolution to $\Delta\omega = \pi/M$. In all practical cases, the performance of two-band filter banks can be improved by increasing the frequency resolution in the low and high frequency region by increasing the number of subbands in the region. We investigate three-band time–frequency localized wavelet filter banks as an alternative that overcomes the limitations of two-band filter banks, without modifying the iterative structure inherent to M-band wavelet filter banks. Three-band filter banks have shown excellent performance in denoising [38] and digital watermarking [39,40] of images. A hybrid of three and two-band filter banks has shown improved performance in image coding [41]. Kokare et al. [42] showed that three-band filter banks outperform two-band filter banks in content based image retrieval. We exploit the flexibility provided by biorthogonal filter banks and design time–frequency localized three-band linear phase biorthogonal wavelet filter banks wherein synthesis scaling and wavelet functions are optimally localized in time and frequency domain.

The Sobolev regularity is used to measure the smoothness or differentiability of the given function [16]. Discontinuous wavelets like Haar with Sobolev regularity of 0.5 [16] cannot detect the singularity in the higher derivatives of the signal [43]. Haar filter banks perform poorly in extracting the features of smooth signals. In this paper, we use finite frequency variance of the scaling function as a sufficient condition that ensures its Sobolev regularity to be more than that of the Haar wavelet [16]. Bhati et al. [16] design time–frequency localized scaling function with unit Sobolev regularity. In this paper, we design the time–frequency localized scaling function with Sobolev regularity of two using a scaling filter with regularity order of two.

Following is the list of contributions of the paper in brief.

- We have proposed a novel sum of time variance and frequency variance based time–frequency uncertainty measure which employs DFT to compute the variance in frequency domain. We have shown that the proposed measure can be used to design time–frequency localized sequences. The proposed DFT based measure exhibits a unique feature that the TFP of the sequence can be arbitrarily minimized by increasing the length of the filter. Note that Sharma et al. [20] and Bhati et al. [35] did the same but DTFT has been used in the methods proposed by them. The UP based on DTFT do not exhibits this property. We have compared TFP of our designed filter with that of the filter designed using Slepian's measure by increasing the energy of the time-limited filter in the given bandwidth [14]. It is found that our proposed measure outperform Slepian's measure [14].
- To the best of our knowledge, none of the authors till date studied the time–frequency localization of scaling function with respect to time–frequency localization of scaling filter in multiresolution setting. In our work, we have shown that the proposed time–frequency localized low pass scaling filter with regularity order of two generates time–frequency localized low pass scaling function with Sobolev regularity of two whose time–frequency localization can be arbitrarily minimized by increasing the length of the filter.
- Bhati et al. [16] designed time–frequency localized three-band orthogonal wavelet filter banks. In this work, we designed time–frequency localized three-band biorthogonal wavelet filter banks. In this work, we have used the expressions for time-center, frequency center, time-variance and frequency variance proposed by Bhati et. al. [16] and design time–frequency localized three band biorthogonal wavelet filter banks with unit Sobolev regularity.
- We have evaluated the performance of our designed three band time–frequency localized filter banks in seizure and seizure-free EEG signals classification. It is found that our designed filter bank outperforms many other methods proposed for seizure and seizure-free EEG signals classification.

The proposed method for the design of three-band BOLP wavelet filter bank has following features:

1. We exploit the flexibility provided by BOLP filter banks to obtain time–frequency localization better than the orthogonal filter banks.
2. Frequency variance of the analysis scaling function can be chosen arbitrarily.
3. It ensures unit Sobolev regularity of the time–frequency localized synthesis scaling function.
4. Admissible wavelets comparable to Morlet and Mexican-hat wavelets can be generated using the proposed design method.
5. To enhance the speed of convergence of the optimization, perfect reconstruction and necessary constraints for regularity are imposed structurally.
6. Bhati et al. [35] employ the biorthogonal linear phase perfect reconstruction filter bank (BOLPPRFB) based on M-Band filter bank lattice structure proposed by Xu and Makur [44]. In order to design time-frequency localized three-band BOLP wavelet filter bank, we have employed the expressions for time and frequency centres and time and frequency variances proposed by Bhati et al. [35]. Three-band filter bank can be replaced by an M-band lattice filter bank and time–frequency localized M-band filter bank can be designed using the proposed method for time–frequency localization.

Assume $G(\Omega)$ is the Fourier transform of a real function $g(t)$ and $E = ||g(t)||_2^2$ represents its energy. The frequency variance $\hat{\triangle}_\Omega^2$ of $g(t)$ and time variance $\hat{\triangle}_t^2$ and frequency center m_Ω and time center m_t of signal $g(t)$ are defined as follows [33,45]:

$$m_t[g(t)] = \frac{1}{||g(t)||^2} \int_{t=-\infty}^{\infty} t|g(t)|^2 dt \tag{1}$$

$$\hat{\triangle}_t^2[g(t)] = \frac{1}{||g(t)||^2} \int_{t=-\infty}^{\infty} |(t-m_t)g(t)|^2 dt \tag{2}$$

$$\triangle_t^2[g(t)] = \frac{1}{||g(t)||^2} \int_{t=-\infty}^{\infty} |tg(t)|^2 dt \tag{3}$$

$$m_\Omega[g(t)] = \frac{1}{\pi||g(t)||^2} \int_{\Omega=0}^{\infty} \Omega|G(\Omega)|^2 d\Omega \tag{4}$$

$$\hat{\triangle}_\Omega^2[g(t)] = \frac{1}{\pi||g(t)||^2} \int_{\Omega=0}^{\infty} |(\Omega-m_\Omega)G(\Omega)|^2 d\Omega \tag{5}$$

$$\triangle_{\Omega}^{2}[g(t)] = \frac{1}{2\pi ||g(t)||^2} \int_{\Omega=-\infty}^{\infty} |\Omega G(\Omega)|^2 d\Omega \tag{6}$$

Here,

$$\hat{\triangle}_{t}^{2}[g(t)] = \triangle_{t}^{2}[g(t)] - m_{t}^{2}[g(t)] \tag{7}$$

$$\hat{\triangle}_{\Omega}^{2}[g(t)] = \triangle_{\Omega}^{2}[g(t)] - m_{\Omega}^{2}[g(t)] \tag{8}$$

In this paper, four cascade iterations are used to generate the scaling function and wavelet functions from the filters of the filter bank. For more details on computing the iterated scaling and wavelet function from the filters and computing its variances in time domain and frequency domain, readers can refer previous work [16]. We use the notation $\hat{\triangle}_{t}^{2'}\hat{\triangle}_{\Omega}^{2'}(h_0[n])$ to denote the product of variances of iterated scaling function generated from the low pass filter $h_0[n]$ [16]. Note that wavelet function is generated by cascade iterations of low pass filter $h_0[n]$ and band pass or high pass filter $h[n]$. Therefore, the notation $\hat{\triangle}_{t}^{2'}\hat{\triangle}_{\Omega}^{2'}(h_0[n], h[n])$ is used to denote the product of variances of the iterated wavelet function [16].

The rest of the paper is organized as follows. In Section 2, we design regular discrete prolate spheroid sequences (DPSS). A technique to impose the regularity of the DPSS is explained. UP for linear operators is explained in the Section 3. In this section, we express the frequency variance of the filter from its DFT and derive the sum based time–frequency uncertainty measure with lower bound of one. An eigenfilter approach is employed in Section 4 and the samples of the time–frequency localized bandlimited scaling and wavelet functions are computed. Time–frequency localized three-band BOLP wavelet PRFB are designed in Section 6. Finally results and discussions, and conclusions are presented in Sections 7 and 8 respectively.

2. Prolate spheroid wave functions

Time–frequency localized filters can be obtained by maximizing the spectral concentration of the time-limited filter in the specified bandwidth $-W < f < W$ where $0 \leq W \leq 0.5$. Such filters are called DPSS [46]. The spectral concentration on the interval $-W \leq f \leq W$ is defined as $\lambda(W) = \frac{\int_{-W}^{W} |H(f)|^2 df}{\int_{-1/2}^{1/2} |H(f)|^2 df}$. In Appendix A, we show that $\lambda(W) = \frac{\mathbf{h}^T \mathbf{J}(W) \mathbf{h}}{\mathbf{h}^T \mathbf{h}}$, where, $\mathbf{J}(W) = \frac{\sin[2\pi W(m-n)]}{\pi(m-n)}$. It can be shown that the matrix $\mathbf{J}(W)$ is positive definite with all of its eigenvalues lying between 0 and 1. The eigenvector corresponding to the maximum eigenvalue is the sequence that maximally concentrates its energy in the bandwidth W. It is also known as 0th order Slepian sequence that maximally suppresses the side-lobes. The matrix $\mathbf{J}(W)$ is ill conditioned with most of its eigenvalues near to one or zero with a narrow transition band [47]. Slepian et al. [46] show that the time-limited DPSS can be obtained by diagonalizing a symmetric tridiagonal matrix. Let N be the length of the filter to be designed and

$$\mathbf{D_N} = \left\{ -\tfrac{N-1}{2},\ -\tfrac{N-3}{2},\ \ldots\ 0,\ \ldots\ \tfrac{N-3}{2},\ \tfrac{N-1}{2} \right\}$$

The symmetric tridiagonal matrix $\mathbf{R}$ is given by the following expressions [47]:

$$R(n,n) = n^2 \cos(2\pi W)$$

$$R(n,n+1) = -\frac{1}{8}(2n+1+N)(2n+1-N)$$

where $n \in \mathbf{D_N}$.

Let $\phi(t)$ and $\psi_k(t)$ represent the scaling and wavelet functions of an M-band wavelet filter bank respectively. Then [2],

$$\phi(t) = \sqrt{M} \sum_{n} h_0[n] \phi(Mt - n) \tag{9}$$

$$\psi_k(t) = \sqrt{M} \sum_{n} h_k[n] \phi(Mt - n) \tag{10}$$

where, $k = 1, 2, .., M-1$. The filters $h_0[n]$ and $h_k[n]$ represent low pass, band pass, and high pass filters of the M-band filter bank. Regularity of a low pass filter is a necessary condition for its cascade iterations for converging to a smooth function $f(t) \in L_2(\Re)$. A K-regular low pass filter of M-band filter bank is typically described by [16]:

$$H_0(z) = \left(\frac{1 + z^{-1} + \ldots.. + z^{-(M-1)}}{M} \right)^K Q(z) \tag{11}$$

where, $Q(z)$ represents the irregular factor of the regular low pass scaling filter $H_0(z)$. We derive the matrix $\mathbf{A}$ to impose the regularity constraint on the scaling filter with scaling factor $M = 2$ and regularity order of K. It is given by:

$$A(k,l) = (-1)^l (l)^{2k} \quad k = 0, 1 \ldots K-1 \quad \text{and} \quad l \in D_N$$

Let the columns of the matrix $\mathbf{U}$ represent the orthogonal basis of the null space of the matrix $\mathbf{A}$. Let $\mathbf{y}$ represents the eigenvector corresponding to the maximum eigenvalue of the matrix $\mathbf{P} = \mathbf{U}^T \mathbf{R} \mathbf{U}$. It should be noted that the optimal time–frequency localized prolate scaling filter $\mathbf{h_0^*}$ with $M = 2$ and regularity order of K can be obtained using the transformation $\mathbf{h_0^*} = \mathbf{U}\mathbf{y}$. Cascade algorithm can be used to obtain the time–frequency localized scaling function $\phi(t)$ from the designed time–frequency localized scaling filter $\mathbf{h_0^*}$.

3. Heisenberg uncertainty principle for linear operators

According to the HUP for linear operators in Hilbert space and arithmetic mean (AM)-geometric mean (GM) inequality [28], we have,

$$\frac{(||\bar{\mathbf{L}}\mathbf{x}||^2 + ||\bar{\mathbf{M}}\mathbf{x}||^2)^2}{4} \geq ||\bar{\mathbf{L}}\mathbf{x}||^2 ||\bar{\mathbf{M}}\mathbf{x}||^2 \geq \frac{1}{4} | < [\mathbf{L}, \mathbf{M}]\mathbf{x}, \mathbf{x} > |^2$$

where, the matrices $\bar{\mathbf{L}}$ and $\bar{\mathbf{M}}$ are the centered counterparts of the Hermitian matrices $\mathbf{L}$ and $\mathbf{M}$ [28]. Let the arguments of the commutator $\mathbf{C} = [\mathbf{L}, \mathbf{M}] = \mathbf{LM} - \mathbf{ML}$ do not commute. Then,

$$\frac{||\mathbf{L}\mathbf{x}||^2}{| < \mathbf{C}\mathbf{x}, \mathbf{x} > |} + \frac{||\mathbf{M}\mathbf{x}||^2}{| < \mathbf{C}\mathbf{x}, \mathbf{x} > |} \geq 1$$

In order to localize the filter $\mathbf{x}$ of length N in time as well as frequency domain simultaneously, we substitute [48,31],

$$\mathbf{M} = j\mathbf{F}^H \mathbf{L} \mathbf{F} \tag{12}$$

$$\mathbf{L} = \text{diag}\left(\left[-\tfrac{N-1}{2},\ -\tfrac{N-3}{2},\ \ldots\ 0,\ \ldots\ \tfrac{N-3}{2},\ \tfrac{N-1}{2} \right] \right) \tag{13}$$

where,

$$\mathbf{F} = \frac{1}{\sqrt{N}} \mathbf{W}_N^{-nk}, \quad \mathbf{W}_N = e^{\frac{j2\pi}{N}} \qquad n, k \in \mathbf{D_N}$$

and minimize the measure $\mathbf{x}^T \mathbf{R} \mathbf{x} = (||\mathbf{L}\mathbf{x}||^2 + ||\mathbf{M}\mathbf{x}||^2)$. The matrix $\mathbf{R} = \mathbf{L^H L} + \mathbf{B}$ is a real symmetric positive definite matrix, where $\mathbf{B} = \mathbf{M}^H \mathbf{M}$. Note that symmetric time–frequency localized filter $\mathbf{x}$ and (12) and (13) imply $\bar{\mathbf{L}} = \mathbf{L}$ and $\bar{\mathbf{M}} = \mathbf{M}$. It should be noted that the measure $\mu_n^2 = \frac{||\mathbf{L}\mathbf{x}||^2}{\mathbf{x}^T \mathbf{x}}$ represents the time variance of the filter $\mathbf{x}$. The frequency variance of the filter can be computed from its DTFT $X(e^{j\omega})$ using following expression [2]:

$$\mu_{\omega}^2 = \frac{1}{2\pi ||x||^2} \int_{-\pi}^{\pi} |\omega X(e^{j\omega})|^2 d\omega \tag{14}$$

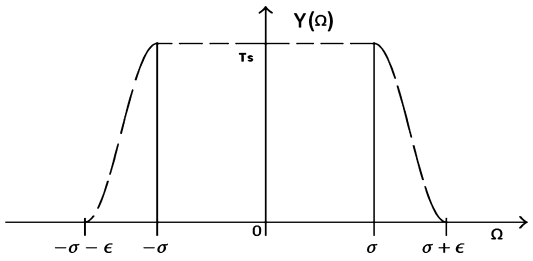

Fig. 1. Fourier transform of bandlimited interpolating function with smooth edges of the box function [16].

It can be shown that the frequency variance of filter is given by $\mu_\omega^2 = \frac{\mathbf{x}^T\mathbf{C}\mathbf{x}}{\mathbf{x}^T\mathbf{x}}$ [25], where,

$$C(m,n) = \begin{cases} \frac{\pi^2}{3} & : \ m = n \\ \frac{2(-1)^{m-n}}{(m-n)^2} & : \ m \neq n \end{cases}$$

The frequency variance of the filter can also be computed from its DFT $X[k]$:

$$X[k] = \frac{1}{\sqrt{N}} \sum_{n=-(N-1)/2}^{(N-1)/2} x[n] W_N^{nk}$$

The frequency variance based on the above expression of $X[k]$ is given by:

$$\mu_k^2 = \frac{1}{||X||^2} \sum_{k=-(N-1)/2}^{(N-1)/2} |kX[k]|^2$$

It can be shown that $\mu_k^2 = \frac{\mathbf{x}^T\mathbf{D}\mathbf{x}}{\mathbf{x}^T\mathbf{x}}$, where,

$$D(m,n) = \frac{1}{N} \sum_{k=-(N-1)/2}^{(N-1)/2} k^2 W_N^{(m-n)k}$$

It should be noted that $\mathbf{D} = \mathbf{B}$. Sharma et al. [31] in their work have not derived the matrix **D**. They employed the notion of quantum harmonic oscillator to obtain the matrix **B**. Let **S** represents the matrix **D** or **C**. The eigenvector of the positive definite matrix $\mathbf{R_S} = \mathbf{L}^H\mathbf{L} + \mathbf{S}$ corresponding to minimum eigenvalue can be used to design time–frequency localized filters subject to specified regularity constraints on the filter **x**. Unlike Sharma et al. [31], we analyze the performance of our proposed time–frequency localization measure in designing regular scaling filters that generate smooth scaling function $\phi(t) \in L_2(\Re)$.

4. Time–frequency localized bandlimited scaling and wavelet functions

Time variance and frequency variance of a bandlimited function can be computed from its samples $f(nT_s)$. Let sampling interval be $T_s < \pi/\sigma$ where σ represents the bandwidth of the interpolating function. Fig. 1 shows the Fourier transform of the interpolating function used by Venkatesh et al. [49] where $\epsilon < \frac{\pi}{T_s} - \sigma$. The samples of the bandlimited function are interpolated and the variances of the interpolated functions are computed. The time variance and frequency variance of the interpolated function are given by [49]:

$$\triangle_t^2(f(kT_s)) = \frac{f(mT_s)^H U_v(m,n) f(nT_s)}{2\pi E} \tag{15}$$

$$\triangle_\Omega^2(f(kT_s)) = \frac{f(mT_s)^H V_v(m,n) f(nT_s)}{2\pi T_s E} \tag{16}$$

where,

$$U_v(m,n) = \frac{m^2+n^2}{2} T_s^2 P(m,n) + Q(m,n)$$

$$P(m,n) = 2\sigma T_s^2 \delta_{mn} + \frac{T_s^2(-1)^{(m-n)}}{2}\left[\epsilon \frac{\sin((m-n)T_s\epsilon)}{(m-n)T_s\epsilon} + \frac{\sin((m-n)T_s\epsilon)}{2} \frac{2(m-n)T_s}{(\frac{\pi}{\epsilon})^2 - (m-n)^2 T_s^2}\right] + \frac{T_s^2(-1)^{(m-n)}}{2}\left[\epsilon \frac{\sin((m-n)T_s\epsilon)}{(m-n)T_s\epsilon}\left(1 - \frac{\frac{1}{2}}{\left[1 - (\frac{(m-n)T_s\epsilon}{2\pi})^2\right]}\right)\right]$$

$$Q(m,n) = \frac{1}{4\epsilon} \frac{\sin((m-n)T_s\epsilon)}{(m-n)T_s\epsilon} \frac{T_s^2\pi^2(-1)^{m-n}}{\left[1 - (\frac{(m-n)T_s\epsilon}{2\pi})^2\right]}$$

$$\sigma = \frac{\pi}{T_s} - \epsilon$$

$$\delta_{mn} = \delta(m-n)$$

and

$$V_v(m,n) = \begin{cases} \frac{2\pi^3}{3} & m = n \\ \frac{4\pi(-1)^{m-n}}{(m-n)^2} & m \neq n \end{cases}$$

Eigenvector of the positive definite matrix $K(m,n) = (U_v(m,n)/2\pi) + V_v(m,n)/(2\pi T_s))$ corresponding to the minimum eigenvalue λ is used to generate the samples of the time–frequency localized bandlimited low pass scaling and band pass wavelet function that minimizes the sum of variances.

5. Time–frequency inequalities

Let $F(j\Omega)$ represents the Fourier transform of the function $f(t) \in L_2(\Re)$. Gabor's UP states that $f(t)$ and $F(j\Omega)$ cannot be arbitrarily localized simultaneously [16]. The uncertainty inequality places a lower bound on the product of effective time and spectral widths of continuous time signals [16]:

$$\triangle_t^2 \triangle_\Omega^2 \geq \frac{1}{4} \tag{17}$$

Using AM-GM inequality, it can be shown that

$$\frac{(\triangle_t^2 + \triangle_\Omega^2)^2}{4} \geq \triangle_t^2 \triangle_\Omega^2 \geq \frac{1}{4} \tag{18}$$

or,

$$(\triangle_t^2 + \triangle_\Omega^2) \geq 1 \tag{19}$$

Similarly $f[n] \in L_2(Z)$ and $F(e^{j\omega})$ cannot be localized arbitrarily and the lower bound on their product is given by [35]:

$$\mu_n^2 \mu_\omega^2 > \frac{(1 - |F_0(e^{j\pi})|^2)^2}{4} \tag{20}$$

Using AM-GM inequality, for the class of sequences $f[n]$ with $F(e^{j\pi}) = 0$, the inequality becomes:

$$\frac{(\mu_n^2 + \mu_\omega^2)^2}{4} \geq \mu_n^2 \mu_\omega^2 > \frac{1}{4}$$

or,

$$(\mu_n^2 + \mu_\omega^2) > 1$$

It should be noted that $(\mu_n^2 + \mu_\omega^2) = \frac{\mathbf{x}^T \mathbf{R_C} \mathbf{x}}{\mathbf{x}^T \mathbf{x}}$ and $(\mu_n^2 + \mu_k^2) = \frac{\mathbf{x}^T \mathbf{R_D} \mathbf{x}}{\mathbf{x}^T \mathbf{x}}$. The matrices $\mathbf{R_C}$ and $\mathbf{R_D}$ are real symmetric and positive definite matrices. Note that, $\mu_n^2 \neq \mu_\omega^2$ and $\mu_n^2 = \mu_k^2$ for the designed time–frequency localized optimal filter. The minimum eigenvalue of the matrix $\mathbf{R_C}$ is one. However, the minimum eigenvalue of the matrix $\mathbf{R_D}$ depends on the length N. In the next section, we formulate an optimization problem to design the three-band, time–frequency localized, BOLP wavelet filter bank.

6. Design of time–frequency localized three-band BOLP wavelet PRFB

Bhati et al. [35] use the parameterized lattice structure to obtain the parameterized filter coefficients of the three-band BOLP wavelet filter bank of length nine and regularity order of one. The free parameters of the filter bank can be optimized for the given optimality criterion and design constraints. In this section, we formulate an optimization problem to design time–frequency localized three-band wavelet filter bank with specified frequency variance of the analysis scaling function. Time–frequency localized smooth synthesis basis functions are desirable for the faithful reconstruction of the local features of the image [50]. We minimize the weighted sum of the TFPs of the synthesis wavelet basis functions for the given frequency variance (θ_v) of the analysis scaling function. Regularity of the analysis and synthesis scaling functions is ensured by imposing a finite upper bound on their frequency variance [16]. It is found that the optimization problem becomes very complex if we impose an upper bound on the time variance of the analysis scaling function. Locating the initial point in the space formed by the free parameters that generate the optimization trajectory towards the optimal point becomes very difficult. Therefore an upper bound on the time variance of the analysis scaling function is not included in the constraint set of the optimization problem. The optimization problem for the design of three-band time–frequency localized BOLP wavelet PRFB can be given by [16]:

$$\mathbf{min}_x(w_{0A}\rho_{0A} + w_{1A}\rho_{1A} + w_{2A}\rho_{2A} + w_{0S}\rho_{0S} + w_{1S}\rho_{1S} + w_{2S}\rho_{2S}) \tag{21}$$

subject to,

$$< h_i[k], f_j[Mn-k] >= \delta[i-j]\delta[n], \quad i,j = 0,1...,M-1 \tag{22}$$

$$H_0(e^{j2\pi/3}) = H_0(e^{j4\pi/3}) = 0 \tag{23}$$

$$F_0(e^{j2\pi/3}) = F_0(e^{j4\pi/3}) = 0 \tag{24}$$

$$H_0(e^{j0}) = \sqrt{3} \tag{25}$$

$$\triangle_\Omega^{2'}(h_0[n]) < \theta_v \tag{26}$$

$$\triangle_\Omega^{2'}(f_0[n]) < \theta_v \tag{27}$$

where,

$$\rho_{0A} = \hat{\triangle}_t^{2'} \triangle_\Omega^{2'}(h_0[n])$$
$$\rho_{1A} = \hat{\triangle}_t^{2'} \hat{\triangle}_\Omega^{2'}(h_0[n], h_1[n])$$
$$\rho_{2A} = \hat{\triangle}_t^{2'} \hat{\triangle}_\Omega^{2'}(h_0[n], h_2[n])$$
$$\rho_{0S} = \hat{\triangle}_t^{2'} \triangle_\Omega^{2'}(f_0[n])$$
$$\rho_{1S} = \hat{\triangle}_t^{2'} \hat{\triangle}_\Omega^{2'}(f_0[n], f_1[n])$$
$$\rho_{2S} = \hat{\triangle}_t^{2'} \hat{\triangle}_\Omega^{2'}(f_0[n], f_2[n])$$
$$x = [h_0[n], h_1[n], h_2[n], f_0[n], f_1[n], f_2[n]]$$

Constraint (22) ensures perfect reconstruction [2]. Constraints (22) to (25) imply $F_0(e^{j0}) = \sqrt{3}$ [2]. The regularity constraints (23), (24), and (25) are necessary for the convergence of the cascade iterations of scaling filter to a smooth function $f(t) \in L_2(\Re)$ [51]. The orthogonal filter bank structure chosen by Bhati et al. [16] exhibits a property that minimizing the weighted sum of TFPs minimize the frequency variance of the scaling function. However, minimizing the weighted sum of TFPs of wavelets and scaling functions of the biorthogonal parameterized lattice filter bank structure chosen in this paper does not minimize the frequency variance of scaling function. Therefore, the constraints of finite frequency variance of the analysis and synthesis scaling functions are imposed explicitly using (26) and (27), respectively. We have used *fminunc* and *fmincon* functions of the optimization toolbox of Matlab software to solve the optimization problems. For more details on the solution of nonlinear constrained optimization problems, reader is suggested to refer the work of Nocedal and Wright [52].

Table 1
Time–frequency localized low pass scaling filters $h_{\mathrm{PSWF}}[n]$ and $h_{\mathrm{RS}}[n]$ with regularity order of two designed by maximizing energy in the specified bandwidth and HUP, respectively. Note that impulse responses $h_{\mathbf{RD}}$ and $h_{\mathbf{RB}}$ are same.

$h_{\mathrm{PSWF}}[n]$	$h_{\mathrm{RD}}[n]$	$h_{\mathrm{RC}}[n]$
0.003496814332297	0.000053844050900	−0.003165552121674
0.023829187324007	0.004520270245653	0.001967747471416
0.079963949038644	0.032652378731613	0.006312842841858
0.173980382423362	0.135935088434331	0.074149730716326
0.270092627222333	0.320847167810761	0.350406099873090
0.311487641691810	0.426196063826580	0.554871824811065
0.270092627222332	0.320847167810762	0.350406099873090
0.173980382423361	0.135935088434331	0.074149730716326
0.079963949038643	0.032652378731613	0.006312842841858
0.023829187324007	0.004520270245653	0.001967747471415
0.003496814332297	0.000053844050899	−0.003165552121674

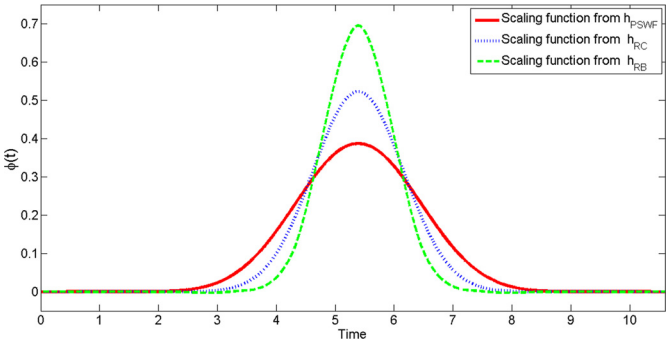

Fig. 2. Sum normalized time–frequency localized scaling functions with $K = 2$.

7. Results and discussion

Time–frequency localized and time-limited scaling filters $h_{\mathrm{PSWF}}[n]$ and $h_{\mathrm{RS}}[n]$ of lengths $N = 11$ and $N = 21$ with scaling factor $M = 2$ and regularity order of $K = 2$ are designed by maximizing their energy in the bandwidth $W = 0.3$ and UP for linear operators respectively. The filter coefficients of the designed sum normalized scaling filters $(H_0(e^{j0}) = \sqrt{2})$ are given in the Table 1. The scaling and wavelet functions generated from the scaling filters $h_{\mathrm{PSWF}}[n]$ and $h_{\mathrm{RS}}[n]$ are shown in the Figs. 2 and 3, respectively. The filter $h_{\mathbf{RS}}[n]$ has been designed using the matrix positive semidefinite matrix $\mathbf{R_S}$. The samples of the wavelet function are generated by convolving the iterated scaling filter with the filter $H(z) = 1 - z^{-1}$ [53]. It can be verified from the eigenvalues of the transition matrix generated by the designed scaling filters that their cascade iterations converge to smooth functions $f(t) \in L_2(\Re)$ with Sobolev regularity $s_{\max} = 2$ [54]. The TFP of the designed scaling filters, scaling functions, and wavelet functions are given in the Tables 2 and 3. It should be noted that even with the regularity order of $K = 0$, the optimal filter obtained from the proposed sum based

Table 2
Comparison of TFP of time–frequency localized scaling filters ($h_0[n]$), scaling functions ($\phi(t)$) and wavelet functions ($\psi(t)$) obtained from the filters $h_{\mathrm{PSWF}}[n]$ and $h_{\mathrm{RS}}[n]$ of length $N = 11$ and $K = 2$.

	$(\mu_n^2\mu_\omega^2)$	$\triangle_t^2(\phi(kT_s))\triangle_\Omega^2(\phi(kT_s))$	$\triangle_t^2(\psi(kT_s))\triangle_\Omega^2(\psi(kT_s))$
$h_{\mathrm{PSWF}}[n]$	0.251031406734349	0.250373906312654	0.316691813106526
$h_{\mathrm{RD}}[n]$	0.250008621275046	0.250002078410343	0.337531010282116
$h_{\mathrm{RC}}[n]$	0.251755721806645	0.250927334136461	0.411560484384427

Table 3
Comparison of TFP of time–frequency localized scaling filters ($h_0[n]$), scaling functions ($\phi(t)$) and wavelet functions ($\psi(t)$) obtained from the filters $h_{\mathrm{PSWF}}[n]$ and $h_{\mathrm{RS}}[n]$ of length $N = 21$ and $K = 2$.

	$(\mu_n^2\mu_\omega^2)$	$\triangle_t^2(\phi(kT_s))\triangle_\Omega^2(\phi(kT_s))$	$\triangle_t^2(\psi(kT_s))\triangle_\Omega^2(\psi(kT_s))$
$h_{\mathrm{PSWF}}[n]$	0.250235667872166	0.250085152884069	0.330741508586166
$h_{\mathrm{RD}}[n]$	0.250000000002000	0.250000000000531	0.339447566992224
$h_{\mathrm{RC}}[n]$	0.250642741010574	0.251248927269165	0.594882890537402

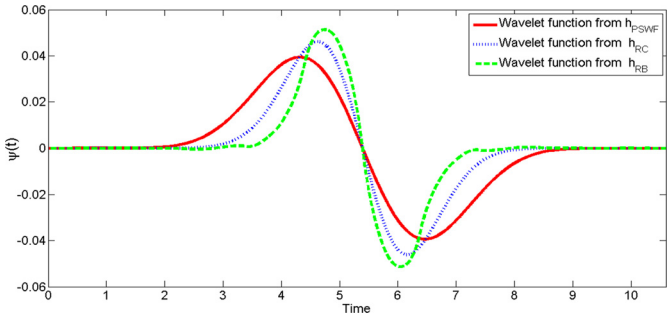

Fig. 3. Energy normalized time–frequency localized wavelet functions with $K = 2$. It should be noted that the impulse response $h_{\mathbf{RD}}$ is similar to impulse response $h_{\mathbf{RB}}$.

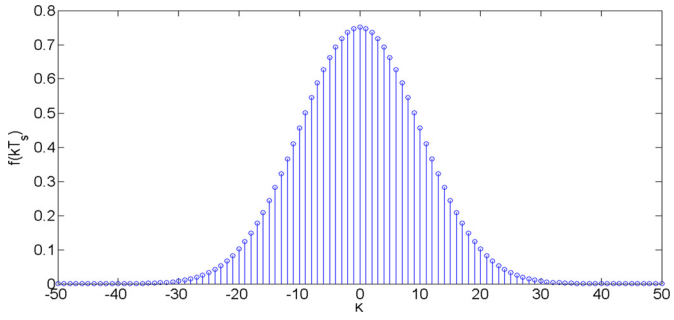

Fig. 4. Samples of time–frequency optimal, low pass, bandlimited scaling function.

uncertainty measure corresponding to the positive definite matrix $\mathbf{R_D}$ is not a Kronecker delta sequence with TFP of zero. The TFP of the filter is found to be 0.25001. Tables 2 and 3 show that uncertainty product can be arbitrarily minimized using the proposed summation based uncertainty measure by increasing the length of the filter N. The results are given for filter lengths $N = 11$ and $N = 21$. It should be noted that increasing the filter length minimizes the product of time variance and frequency variance when DFT based measure is used for time–frequency localization. However, this property does not hold for other measures used for time–frequency localization. Since, the designed filter with $K = 0$ is not a regular filter, the corresponding scaling and wavelet functions do not exist.

The samples of the time–frequency localized, bandlimited low pass scaling and bandpass wavelet function $f(t)$ with $T_s = 0.1$ are obtained from the eigenvector of the positive definite matrix $\mathbf{K}$. It is assumed that the samples $f(kT_s)$ are centered at $k = 0$ with odd number of samples $L = 101$. Then $f(kT_s) \in \mathbb{R}^L$, and $U_v(m,n) \in \mathbb{R}^{L\times L}$, and $V_v(m,n) \in \mathbb{R}^{L\times L}$.

Let

$$\sigma_t^2 = \frac{f(mT_s)^H U_v(m,n) f(nT_s)}{2\pi}$$

$$\sigma_\Omega^2 = \frac{f(mT_s)^H V_v(m,n) f(nT_s)}{2\pi T_s}$$

and

$$E = T_s\big(f(mT_s)^H f(nT_s)\big)$$

Note that $\triangle_t^2(f(kT_s)) = \frac{\sigma_t^2}{E}$ and $\triangle_\Omega^2(f(kT_s)) = \frac{\sigma_\Omega^2}{E}$. Eigenvector of the matrix $K(m,n) = (U_v(m,n)/(2\pi) + V_v(m,n)/(2\pi T_s))$ corresponding to the minimum eigenvalue λ generates the samples of the bandlimited low pass scaling function that minimizes $\sigma_t^2 + \sigma_\Omega^2$. Fig. 4 shows the samples $f(nT_s)$ of the normalized low pass scaling function and the minimum value of $\triangle_t^2(f(kT_s)) + \triangle_\Omega^2(f(kT_s)) = (\sigma_t^2 + \sigma_\Omega^2)/E$ is found to be 1. Table 4 and Fig. 5 shows the variation of sum of variances and product of variances for different number of samples (L) of bandlimited function. It shows that the lower bound of sum of variances and product of variances is independent of number of samples for sufficiently large L. The time variance and frequency variance of the designed optimally time–frequency localized scaling function is 0.5. It is found that $F(e^{j\omega_k}) = 0$ for $\omega_k = 2\pi k/L$, where, $k = 1, 2, ..., L-1$ for sufficiently large L and T_s.

We analyzed the minimum eigenvalue λ of $\mathbf{K}$ with respect to length L and sampling time T_s. Fig. 6 shows the plot of λ with respect L for different values of T_s. Note that for $L >> 1$, $\lambda = T_s$.

In order to obtain the samples of the bandlimited band pass wavelet function, the eigenvector of the positive definite matrix $\mathbf{K}$ corresponding to minimum eigenvalue are generated subject to the linear constraint $F(e^{j0}) = 0$. Fig. 7 shows the samples of normalized band pass wavelet function. The minimum value of $\triangle_t^2(f(kT_s)) + \triangle_\Omega^2(f(kT_s))$ is found to be 3 with $\triangle_t^2(f(kT_s)) = 1.5$ and $\triangle_\Omega^2(f(kT_s)) = 1.5$, which is same as that of Gaus1 wavelet [55]. Note that the TFPs of the designed bandlimited scaling and wavelet functions are close the lowest possible lower bounds of 0.25 and 2.25 respectively.

The objective function in the optimization problem (21) is the weighted sum of the TFPs of the analysis and synthesis, wavelet and scaling functions. The perfect reconstruction, regularity and sum-normalization constraints are imposed structurally. However, explicit constraints are formulated to impose upper bound θ_v, on the frequency variance of the scaling functions. It is an optimization problem in which both the objective function and constraints are highly nonlinear. Filter coefficients are obtained from the free parameters and the scaling and wavelet functions are generated. The sum of the weighted TFPs of the functions is minimized with respect to the free parameters of the filter bank. Starting from the initial guess for the free parameters, in each optimization it-

Table 4
Lower bound of the sum and product of variances of time–frequency localized function for different number of samples.

Number of samples (L)	$\triangle_t^2(f(kT_s))\triangle_\Omega^2(f(kT_s))$	$\triangle_t^2(f(kT_s))+\triangle_\Omega^2(f(kT_s))$
10	0.3219	8.5615
20	0.3160	2.4294
30	0.2964	1.3374
40	0.2690	1.0653
50	0.2536	1.0083
60	0.2503	1.0006
70	0.2500	1.0000
80	0.2500	1.0000
90	0.2500	1.0000
100	0.2500	1.0000

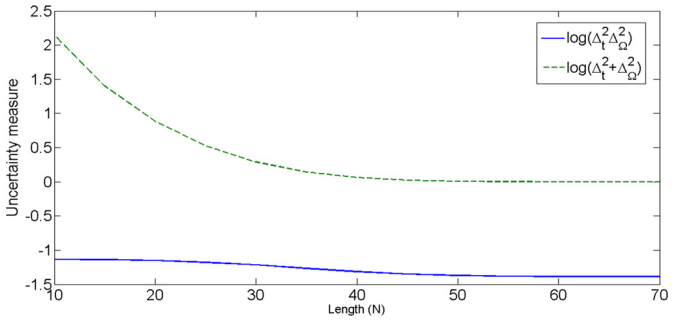

Fig. 5. Comparison of sum of variances and product of variances of time–frequency localized bandlimited function with respect to the number of samples (L).

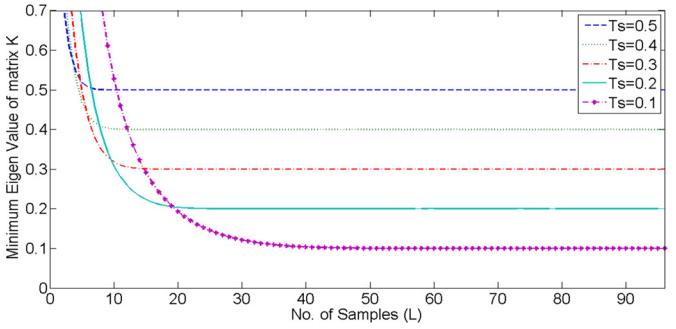

Fig. 6. Minimum eigenvalue of matrix **K** versus L and T_s.

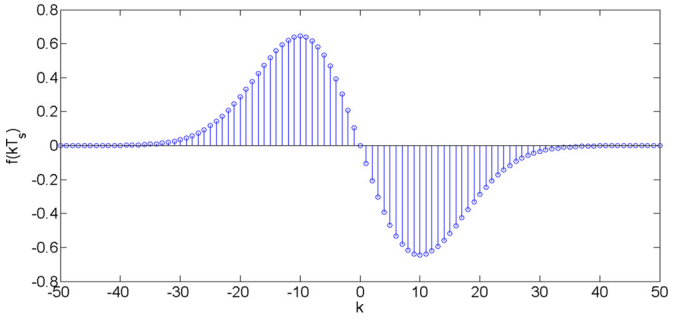

Fig. 7. Samples of time–frequency optimal, band pass, and bandlimited wavelet function.

eration, the seven parameters of the filter bank are optimized to minimize the weighted sum of TFPs [52]. For the given value of θ_v and the weight scheme, several iterations of the optimization are performed to obtain the sufficiently small value of the objective function. Table 5 shows the three weight schemes chosen to formulate the time–frequency objective function to be minimized.

Tables 6 and 7 show the analysis and synthesis filter coefficients of time–frequency localized filter bank, respectively, designed using the weight scheme for case I. Note that all the weights are zero except for the TFPs of the scaling functions. Thus the objective function involves the frequency variance of the scaling functions and the explicit constraint for the upper bound θ_v on the frequency variance is not required. Table 8 shows the values of the TFP of functions for the designed filter bank. Figs. 8 and 9 show the corresponding analysis and synthesis functions respectively. Table 8 shows that the TFP of analysis and synthesis functions are almost same even when the filter coefficients of the analysis and synthesis filter banks are different.

Tables 9 and 10 show the analysis and synthesis filter coefficients of time–frequency localized filter banks designed using the weight scheme given by case II. We choose $\theta_v = 1000$ for the scaling functions to obtain sufficiently large feasible set which eventually leads to the small value of the TFP of the wavelet functions. Table 11 shows the values of the TFP of functions for the optimal filter bank. Figs. 10 and 11 show the corresponding analysis and synthesis functions, respectively. Note that TFP of the analysis and synthesis wavelet functions is minimized in this case and therefore the TFP obtained for the optimal wavelet functions is better than that given in Table 8.

We minimize the TFP of two synthesis wavelets using the weight scheme given by case III. The TFP of synthesis wavelets are assigned equal and nonzero weights and all other weights are zero

Table 5
Weight schemes for the optimization problem in (21).

Case	w_{0A}	w_{0S}	w_{1A}	w_{1S}	w_{2A}	w_{2S}
I	0.5	0.5	0	0	0	0
II	0	0	0.25	0.25	0.25	0.25
III	0	0	0	0.5	0	0.5

Table 6
Case I: Analysis filter bank coefficients.

$h_0[n]$	$h_1[n]$	$h_2[n]$
−0.020331916118530	−0.152851915357923	0.059305610380147
−0.075927743925236	−0.570811969718933	0.221471560871226
0.141773812434708	1.065831604454154	−0.413536158291452
0.455908372873448	0.000027828383033	0.073759363237566
0.729205757040097	0	0.117999247605027
0.455908372873448	−0.000027828383033	0.073759363237566
0.141773812434708	−1.065831604454154	−0.413536158291452
−0.075927743925236	0.570811969718933	0.221471560871226
−0.020331916118530	0.152851915357923	0.059305610380147

Table 7
Case I: Synthesis filter bank coefficients.

$f_0[n]$	$f_1[n]$	$f_2[n]$
−0.020331102710247	0.051456780953350	0.125652483874700
−0.075926927890449	0.192166423661345	0.469251826542672
0.141774261651386	−0.358822009341455	−0.876208653307313
0.455907110248486	0.000009368630281	0.156318059515748
0.729204124970524	0	0.249972566748385
0.455907110248486	−0.000009368630281	0.156318059515748
0.141774261651386	0.358822009341455	−0.876208653307313
−0.075926927890449	−0.192166423661345	0.469251826542672
−0.020331102710247	−0.051456780953350	0.125652483874700

Table 8
TFP of analysis and synthesis functions obtained from the weight scheme given by case I.

Function	TFP	
	Synthesis filter bank	Analysis filter bank
Scaling	0.6947	0.6947
Wavelet1	24.4474	24.4470
Wavelet2	23.1373	23.1368

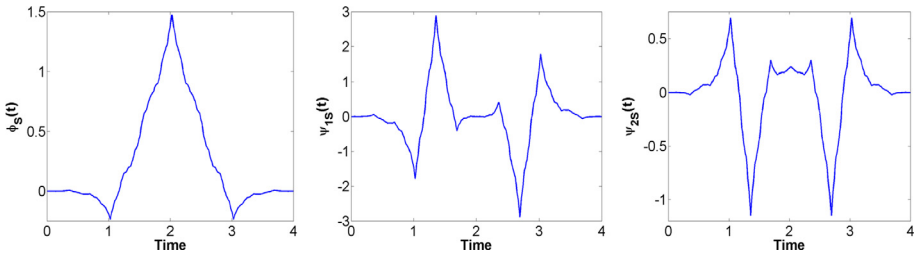

(a) Scaling (b) Wavelet1 (c) Wavelet2

Fig. 8. TFP optimized analysis functions corresponding to the weight scheme given by case I.

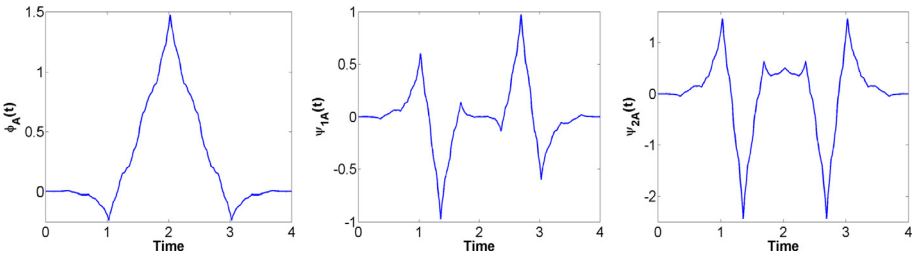

(a) Scaling function (b) Wavelet1 (c) Wavelet2

Fig. 9. TFP optimized synthesis functions corresponding to the weight scheme given by case I.

Table 9
Case II: Analysis filter bank coefficients with $\theta_v = 1000$.

$h_0[n]$	$h_1[n]$	$h_2[n]$
0.017279508134988	−0.137774214043212	−0.101581841073796
−0.038377655752156	0.305995478387950	0.225612494114144
0.142734407569587	−1.138060219434404	−0.839099341962031
0.417336353485051	2.772818145817379	1.598998772190779
0.654105580693937	0	−1.767860166538193
0.417336353485051	−2.772818145817379	1.598998772190779
0.142734407569587	1.138060219434404	−0.839099341962031
−0.038377655752156	−0.305995478387950	0.225612494114144
0.017279508134988	0.137774214043212	−0.101581841073796

Table 10
Case II: Synthesis filter bank coefficients with $\theta_v = 1000$.

$f_0[n]$	$f_1[n]$	$f_2[n]$
−0.044146927330589	0.022246493298586	−0.037682230198930
−0.117250686628542	0.059084896097154	−0.100080971240278
0.104255226268126	−0.052536231460653	0.088988513430583
0.517241970252088	−0.207299607400775	0.201864328358124
0.811851642446709	0	−0.306179280698997
0.517241970252088	0.207299607400775	0.201864328358124
0.104255226268126	0.052536231460653	0.088988513430583
−0.117250686628542	−0.059084896097154	−0.100080971240278
−0.044146927330589	−0.022246493298586	−0.037682230198930

Table 11
TFP of analysis and synthesis functions obtained from weight scheme given by case II.

Function	TFP	
	Synthesis filter bank	Analysis filter bank
Scaling	1.4366	0.7575
Wavelet1	7.9450	8.7015
Wavelet2	11.9062	10.9703

in the weight scheme given by case III. We choose $\theta_v = 1000$ to obtain sufficiently large feasible set to obtain small value of the TFP of analysis scaling and wavelet functions. Tables 12 and 13 show the analysis and synthesis filter coefficients, respectively. Though the synthesis functions are regular having very small values of TFP, the TFP of the analysis functions is relatively large. Figs. 12 and 13 show the analysis and synthesis functions for case III weight scheme in which synthesis wavelets are optimized for TFP with frequency variance of $\theta_v = 1000$ of the analysis function. Note that the wavelet functions in Fig. 13 are admissible and comparable to that of Mexican hat and Morlet wavelets [56]. Table 14 shows the TFPs of the functions of the designed time–frequency optimal filter bank for the fixed values of the frequency variance of the analysis scaling function. The notations scal., wave1 and wave2 denote the scaling and wavelet functions. Tables 15 and 16 give filter coefficients for time–frequency optimal filter bank with fixed frequency variance of 400 of the analysis scaling function. The results show that the proposed design method generates time–frequency localized filter bank with following features:

Table 12
Case III: Analysis filter bank coefficients with $\theta_v = 1000$. It can be noted that scaling function has frequency variance of 1000.

$h_0[n]$	$h_1[n]$	$h_2[n]$
0.010799933538597	−0.003161261939002	0.004075805353696
−0.168853120969085	0.049425206432388	−0.063723767556016
−0.083909065803780	0.024561126706446	−0.031666585577068
0.650459401454808	−0.178773714602571	0.374806248857250
0.915056511127796	0	−0.566983402155723
0.650459401454808	0.178773714602571	0.374806248857250
−0.083909065803780	−0.024561126706446	−0.031666585577068
−0.168853120969085	−0.049425206432388	−0.063723767556016
0.010799933538597	0.003161261939002	0.004075805353696

Table 13
Case III: Synthesis filter bank coefficients with $\theta_v = 1000$.

$f_0[n]$	$f_1[n]$	$f_2[n]$
−0.021501505365988	−0.048252362797027	0.019548644756325
0.021975230199127	0.049315467083237	−0.019979343831466
0.176520991327250	0.396137608499100	−0.160488584066732
0.422330783228365	2.865743169421407	0.620949275652530
0.533399808791372	0	−0.920059985021314
0.422330783228365	−2.865743169421407	0.620949275652530
0.176520991327250	−0.396137608499100	−0.160488584066732
0.021975230199127	−0.049315467083237	−0.019979343831466
−0.021501505365988	0.048252362797027	0.019548644756325

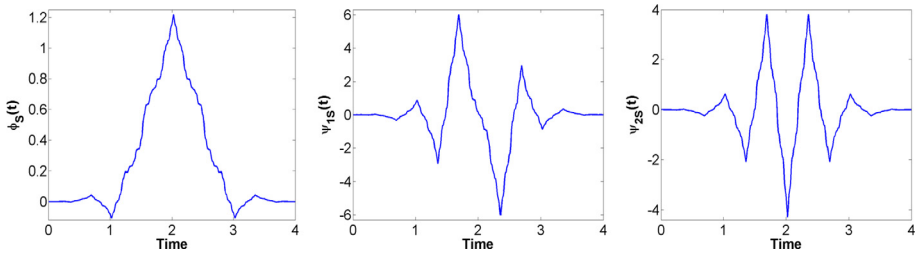

(a) Scaling (b) Wavelet1 (c) Wavelet2

Fig. 10. TFP optimized analysis functions corresponding to the weight scheme given by case II with $\theta_v = 1000$.

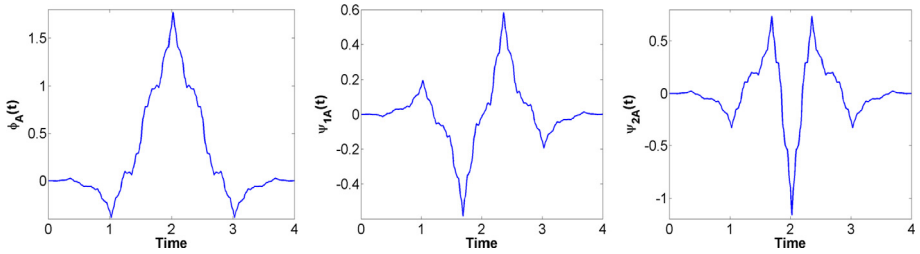

(a) Scaling (b) Wavelet1 (c) Wavelet2

Fig. 11. TFP optimized synthesis functions corresponding to the weight scheme given by case II with $\theta_v = 1000$.

Table 14
TFP and Sobolev regularity of functions for specified frequency variance of the analysis scaling function and the weight scheme given by case III.

Synthesis filter bank			Analysis filter bank			Sobolev regularity of scaling function		$\hat{\triangle}^2_\Omega(\phi_a(t))$
Scal.	Wave1	Wave2	Scal.	Wave1	Wave2	Synthesis	Analysis	
0.627	1.425	2.439	3.846	45.3	27.5	0.985	0.665	50
0.585	1.283	1.298	7.850	65.0	39.7	0.982	0.591	100
0.483	1.057	0.744	16.493	93.7	59.6	0.988	0.513	200
0.278	0.522	0.430	46.306	137.2	56.9	0.999	0.353	400
0.266	0.469	0.344	150.587	237.9	92.6	0.999	0.209	1000

Table 15
Case III : Analysis filter bank coefficients with $\theta_v = 400$. It can be noted that scaling function has frequency variance of 400.

$h_0[n]$	$h_1[n]$	$h_2[n]$
0.003146976916281	−0.001299522590878	0.001340262044756
−0.146538283107354	0.060511981623150	−0.062409005269904
−0.026718913157296	0.011033392419238	−0.011379284352732
0.600922205430640	−0.191702756375154	0.309716513400795
0.870426835404332	0	−0.474536971645829
0.600922205430640	0.191702756375154	0.309716513400795
−0.026718913157296	−0.011033392419238	−0.011379284352732
−0.146538283107354	−0.060511981623150	−0.062409005269904
0.003146976916281	0.001299522590878	0.001340262044756

Table 16
Case III: Synthesis filter bank coefficients with $\theta_v = 400$.

$f_0[n]$	$f_1[n]$	$f_1[n]$
−0.029086671389196	−0.024655867629929	0.044389995734981
0.008947547515711	0.007584558033746	−0.013655106517567
0.169684754066125	0.143836494010983	−0.258960724948557
0.436752186512696	2.619044250951849	0.770724166226453
0.559455174158205	0	−1.084996660990620
0.436752186512696	−2.619044250951849	0.770724166226453
0.169684754066125	−0.143836494010983	−0.258960724948557
0.008947547515711	−0.007584558033746	−0.013655106517567
−0.029086671389196	0.024655867629929	0.044389995734981

- Filter banks with prescribed frequency variance of the analysis scaling function.
- Synthesis wavelet functions are optimally localized in time and frequency domains.
- Unit Sobolev regularity of the synthesis scaling function.
- Wavelet functions are admissible and comparable to that of Mexican hat and Morlet wavelets.

We further evaluate the performance of the designed filter bank in seizure and seizure-free EEG signals classification. We have used seizure and seizure-free EEG signals from the (S) and (N,F) classes of EEG signal dataset from Bonn university, Germany [57]. The signals from N and F classes are combined to form a set of 200 seizure-free EEG signals and 100 EEG signals from class S are used as seizure EEG signals [58]. Fig. 14 shows the samples of EEG signals from each of the S, F and N classes. Readers are suggested to refer to the work of Andrzejak et al. [57] for more details of the dataset. For fair comparative analysis, we have chosen the classification method, simulation parameters and classifier used by Bhati et al. [35]. They evaluate the performance of the proposed filter banks using multilayer perceptron neural network (MLPNN) classifier for the set of EEG signals from Bonn university database [57]. In this work, similar to the work of Bhati et al. [35], we have used ten-fold cross validation for performance evaluation [59]. Bhati et al. [35] have provided a Matlab code to describe the simulation environment and the parameters used for performance evaluation. In this work, we have used the same simulation model, EEG signals and the attributes of the MLPNN and evaluate the performance of three band synthesis filter bank given in Table 13 at the third level of wavelet decomposition. Table 17 compares the classification accuracies of various methods for EEG signals of seizure

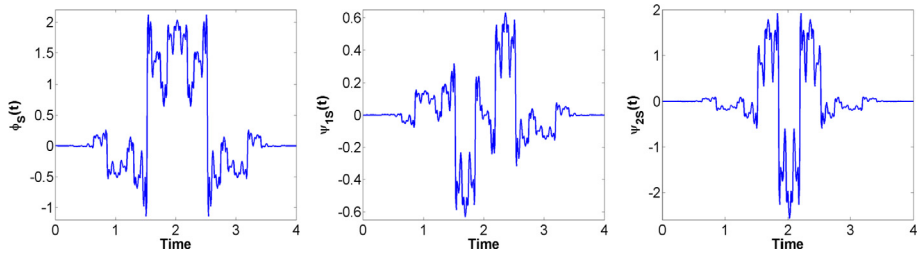

Fig. 12. TFP optimized analysis functions corresponding to the weight scheme given by case III with $\theta_v = 1000$.

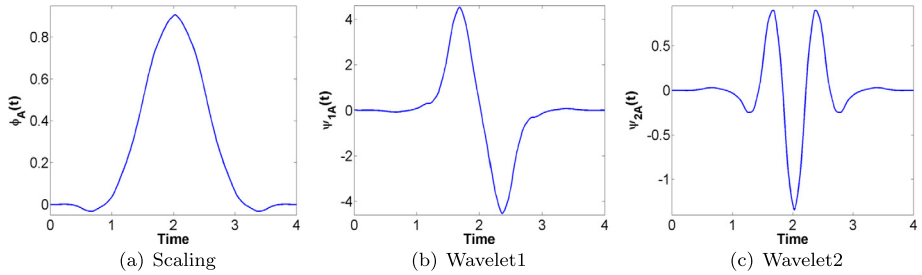

Fig. 13. TFP optimized synthesis functions corresponding to the weight scheme given by case III with $\theta_v = 1000$.

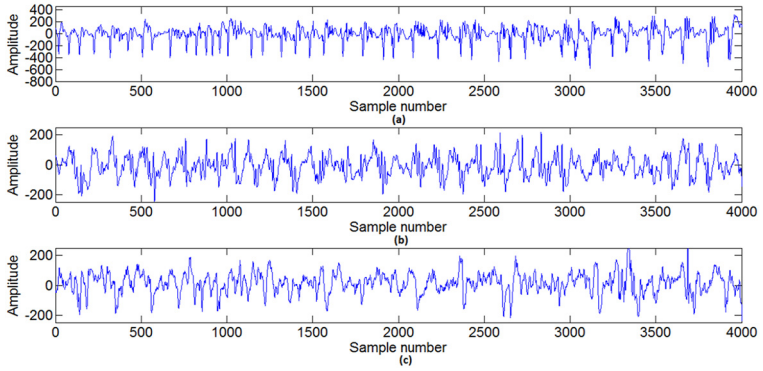

Fig. 14. Plot of EEG signals (a) seizure signal EEG (class S) (b) seizure-free EEG signal (class F) and (c) seizure-free EEG signal (class N).

Table 17
Comparison of classification accuracies (%) of designed filter bank with existing methods for seizure (S) and seizure-free (F, N) EEG signals.

Reference, Year	Signal analysis techniques and studied features	Used classifier	Obtained classification accuracy (%)
[60], 2008	Power spectral density analysis and Petrosian fractal dimension and Higuchi fractal dimension, Hjorth parameters	Probabilistic neural network	97
[61], 2010	Linear prediction and energy of prediction error signal	Error energy based classification	94
[62], 2014	Fractional linear prediction and modeling error energy	support vector machine	95.33
[63], 2014	Second-order difference plot (SODP) of intrinsic mode functions and 95% confidence ellipse area measured from the SODP	Multilayer perceptron neural network	97.75
[64], 2014	Phase space representation (PSR) of intrinsic mode functions and combination of 95% confidence ellipse area for 2D PSR and interquartile range	Least squares support vector machine	98.67
[65], 2015	Local binary patterns and histogram matching scores	Nearest neighbor classifier	98.33
[66], 2016	Key-point based local binary pattern and histogram of local binary pattern	support vector machine	99.45
[35], 2016	Time–frequency localized three-band analysis and synthesis filter banks and subband norm	Multilayer perceptron neural network	99.33
[67], 2017	Tunable-Q wavelet transform and multi-scale K-nearest neighbour entropy measure	support vector machine	99.5
[68], 2017	Analytic time–frequency flexible wavelet transform and fractal dimension of subband signals	Least squares support vector machine	98.67
This work	Time–frequency localized three-band synthesis wavelet filter bank and subband norm	Multilayer perceptron neural network	99.66

and seizure-free categories. It shows that the proposed three band time–frequency localized filter bank performs better than various other methods recently proposed in the literature for seizure and seizure-free EEG signals classification.

8. Conclusion

We have used DFT and DTFT to compute the frequency variance of a filter. The sum of time variance and frequency variance is used to formulate a summation based uncertainty measure and it is minimized to design the time–frequency localized filter which is simultaneously localized in time and frequency domains. Employing the sum of variances in place of product of variances reduces the nonlinearity of the time–frequency optimization problem. Sum of variances facilitates the problem formulation as eigenvalue problem and globally optimal solutions can be computed from the associated eigenvalues and eigenvectors. It is found that the proposed time–frequency localized filter designed using DFT has lower uncertainty product than the filter designed using the summation based uncertainty measure that employ DTFT or by maximizing the energy in given bandwidth. It is also found that the scaling function generated from the cascade iterations of the proposed time–frequency localized low pass filter is even more localized in time and frequency domain than the scaling functions generated from the time–frequency localized scaling low pass filters obtained from the DTFT based frequency measure or maximizing the energy in the given bandwidth. It should be noted that uncertainty product can be arbitrarily minimized using the proposed summation based uncertainty measure by increasing the length of the filter to be designed. We provide sufficient examples in the paper to show that this property is exhibited only by the proposed summation and DFT based uncertainty measure and therefore it can be considered as discrete-time equivalent of continuous time uncertainty measure proposed by Gabor. We have proposed a novel method for time–frequency localization of a regular scaling filter and scaling function. The proposed method outperforms Slepian's, Ishii and Furukawa's methods for time–frequency localization. Time–frequency localized three-band BOLP wavelet filter banks with prescribed frequency variance of the analysis scaling function are designed. The designed time–frequency localized three-band filter bank is shown to outperform in seizure and seizure-free EEG signals classification than the other existing methods.

Acknowledgments

The authors acknowledge the support received from the Bharti Center for Communication, Department of Electrical Engineering, Indian Institute of Technology (IIT) Bombay; from the 'Knowledge Incubation under TEQIP' Initiative of the Ministry for Human Resource Development (MHRD) at IIT Bombay; from the research group associated with Dr. Ram Bilas Pachori at IIT Indore and from Acropolis Institute of Technology and Research, Indore towards the research work carried out and reported in this manuscript.

Appendix A

Expression for energy in the given bandwidth for time-limited filters. Let,

$$E = \mathbf{h}^H \mathbf{h}$$

Then,

$$E = \sum_{n=-\infty}^{\infty} h[n]h^*[n]$$

$$E = \sum_{n=-\infty}^{\infty} h[n]\left(\int_{-1/2}^{1/2} H(f)e^{j2\pi fn}df\right)^*$$

$$E = \sum_{n=-\infty}^{\infty} h[n]\left(\int_{-1/2}^{1/2} H^*(f)e^{-j2\pi fn}df\right)$$

$$E = \int_{-1/2}^{1/2} H^*(f)\left(\sum_{n=-\infty}^{\infty} h[n]e^{-j2\pi fn}\right)df$$

$$E = \int_{-1/2}^{1/2} H^*(f)H(f)df$$

$$E = \int_{-1/2}^{1/2} |H(f)|^2 df$$

Let,

$$\lambda(W) = \frac{\int_{-W}^{W} H(f)H^*(f)df}{E}$$

$$\lambda(W) = \frac{\int_{-W}^{W}\left(\sum_{n=-\infty}^{\infty} h[n]e^{-j2\pi fn}\right)\left(\sum_{m=-\infty}^{\infty} h[m]e^{-j2\pi fm}\right)^* df}{E}$$

$$\lambda(W) = \frac{\sum_{n=-\infty}^{\infty}\sum_{m=-\infty}^{\infty} h[n]h^*[m]\int_{-W}^{W} e^{j2\pi f(m-n)}df}{E}$$

Note that

$$\int_{-W}^{W} e^{j2\pi f(m-n)}df = \frac{\sin(2\pi W(m-n))}{\pi(m-n)}$$

Let,

$$\mathbf{J} = \frac{\sin(2\pi W(m-n))}{\pi(m-n)}$$

Then,

$$\lambda(W) = \frac{\mathbf{h}^T\mathbf{J}(W)\mathbf{h}}{\mathbf{h}^T\mathbf{h}}$$

References

[1] S. Mallat, A Wavelet Tour of Signal Processing, second ed., 1999.
[2] M. Vetterli, J. Kovacevic, Wavelets and Subband Coding, Signal Processing Series, Prentice Hall, Englewood Cliffs, NJ, 1995.
[3] G. Strang, T. Nguyen, Wavelets and Filter Banks, Wellesley Cambridge Press, 1996.
[4] S. Blanco, S. Kochen, O. Rosso, P. Salgado, Applying time–frequency analysis to seizure EEG activity, IEEE Eng. Med. Biol. Mag. 16 (1) (1997) 64–71.
[5] D. Gabor, Theory of communication, Proc. Inst. Electr. Eng. 93 (26) (1946) 429–441.
[6] C.K. Chui, H. Mhaskar, Signal decomposition and analysis via extraction of frequencies, Appl. Comput. Harmon. Anal. 40 (1) (2016) 97–136.
[7] M. Sharma, A. Dhere, R.B. Pachori, V.M. Gadre, Optimal duration-bandwidth localized antisymmetric biorthogonal wavelet filters, Signal Process. 134 (2017) 87–99.
[8] D.M. Monro, B.G. Sherlock, Space-frequency balance in biorthogonal wavelets, in: IEEE International Conference on Image Processing, 1997, pp. 624–627.

[9] L. Shen, Z. Shen, Compression with time–frequency localization filters, in: G. Chen, M. Lai (Eds.), Wavelets and Splines, Athens, Nashboro Press, 2006, pp. 428–443.
[10] D.M. Monro, B. Bassil, G. Dickson, Orthonormal wavelets with balanced uncertainty, in: Proceedings of International Conference on Image Processing, Lausanne, Switzerland, vol. 1, 1996, pp. 581–584.
[11] R. Wilson, Uncertainty, eigenvalue problems and filter design, in: International Conference on Acoustics Speech and Signal Processing, San Diego, California, USA, vol. 9, 1984, pp. 164–167.
[12] R. Wilson, G.H. Granlund, The uncertainty principle in image processing, IEEE Trans. Pattern Anal. Mach. Intell. 6 (6) (1984) 758–767.
[13] C. Herley, J. Kovačević, K. Ramchandran, M. Vetterli, Tilings of the time–frequency plane: construction of arbitrary orthogonal bases and fast tiling algorithms, IEEE Trans. Signal Process. 41 (Dec. 1993) 3341–3359.
[14] D. Slepian, H.O. Pollak, Prolate spheroidal wave function, Fourier analysis and uncertainty-I, Bell Syst. Tech. J. 40 (1) (1961) 43–63.
[15] R. Ishii, K. Furukawa, The uncertainty principle in discrete signals, IEEE Trans. Circuits Syst. 33 (1986) 1032–1034.
[16] D. Bhati, M. Sharma, R.B. Pachori, S.S. Nair, V.M. Gadre, Design of time–frequency optimal three-band wavelet filter banks with unit Sobolev regularity using frequency domain sampling, Circuits Syst. Signal Process. 35 (12) (2016) 4501–4531.
[17] R. Kolte, P. Patwardhan, V.M. Gadre, A class of time–frequency product optimized biorthogonal wavelet filter banks, in: National Conference on Communications, Jan. 2010, pp. 1–5.
[18] M. Sharma, R. Kolte, P. Patwardhan, V.M. Gadre, Time–frequency localization optimized biorthogonal wavelets, in: International Conference on Signal Processing and Communications, July 2010, pp. 1–5.
[19] H. Xie, J.M. Morris, Design of orthonormal wavelets with better time–frequency resolution, Proc. SPIE 2242 (1994) 878–887.
[20] M. Sharma, V.M. Gadre, S. Porwal, An eigenfilter-based approach to the design of time–frequency localization optimized two-channel linear phase biorthogonal filter banks, Circuits Syst. Signal Process. 34 (3) (2015) 931–959.
[21] D.B. Tay, Balanced-uncertainty optimized wavelet filters with prescribed regularity, in: International Symposium on Circuits and Systems, Scottsdale, Arizona, 1999, pp. 532–535.
[22] D.B. Tay, Balanced-uncertainty optimized wavelet filters with prescribed vanishing moments, Circuits Syst. Signal Process. 23 (2) (2004) 105–121.
[23] P. Tay, J. Havlicek, V. DeBrunner, A wavelet filter bank which minimizes a novel translation invariant discrete uncertainty measure, in: Fifth IEEE Southwest Symposium on Image Analysis and Interpretation, 2002, pp. 173–177.
[24] L. Maccone, A.K. Pati, Stronger uncertainty relations for all incompatible observables, Phys. Rev. Lett. 113 (26) (2014) 260.
[25] Y. Venkatesh, K.S. Raja, V.G. Sagar, On bandlimited signals with minimal space/time-bandwidth product, in: IEEE International Conference on Multimedia and Expo, 2004.
[26] C.K. Chui, J. Wang, A study of asymptotically optimal time–frequency localization by scaling functions and wavelets, Ann. Numer. Math. 4 (1996) 193–216.
[27] S. Nam, An uncertainty principle for discrete signals, in: SampTA, 2013.
[28] R. Parhizkar, Y. Barbotin, M. Vetterli, Sequences with minimal time–frequency uncertainty, Appl. Comput. Harmon. Anal. 38 (3) (2015) 452–468.
[29] E.A. Lebedeva, J. Prestin, Periodic wavelet frames and time–frequency localization, Appl. Comput. Harmon. Anal. 37 (2) (2014) 347–359.
[30] M. Sharma, D. Bhati, S. Pillai, R.B. Pachori, V.M. Gadre, Design of time–frequency localized filter banks: transforming non-convex problem into convex via semidefinite relaxation technique, Circuits Syst. Signal Process. 35 (10) (2016) 3716–3733.
[31] M. Sharma, New Approaches for the Design of Filter Banks and Discrete Sequences Based on Uncertainty Measures, Ph.D. Thesis, Indian Institute of Technology, Bombay, Mumbai, India, 2015.
[32] J. Prestin, E. Quak, H. Rauhut, K. Selig, On the connection of uncertainty principles for functions on the circle and on the real line, J. Fourier Anal. Appl. 9 (4) (2003) 387–409.
[33] M. Vetterli, J. Kovačević, V.K. Goyal, Foundations of Signal Processing, Cambridge University Press, 2014.
[34] L. Debnath, F.A. Shah, Wavelet Transforms and Their Applications, Springer, 2002.
[35] D. Bhati, M. Sharma, R.B. Pachori, V.M. Gadre, Time–frequency localized three-band biorthogonal wavelet filter bank using semidefinite relaxation and nonlinear least squares with epileptic seizure EEG signal classification, Digit. Signal Process. 62 (2017) 259–273.
[36] B. Boashash, Time–Frequency Signal Analysis and Processing: A Comprehensive Reference, Academic Press, 2015.
[37] A.N. Akansu, R.A. Haddad, Multiresolution Signal Decomposition: Transforms, Subbands, and Wavelets, Academic Press, Inc., 1992.
[38] P. Zhao, C. Zhao, Three-channel symmetric tight frame wavelet design method, Inf. Technol. J. 12 (2013) 623–631.
[39] G. Bhokare, A.K. Bhardwaj, N. Rai, V.M. Gadre, Digital watermarking with 3-band filter banks, in: Proceedings of the Fourteenth National Conference on Communications, 2008, pp. 466–470.
[40] A. John, V.M. Gadre, C. Gupta, Digital watermarking with 3-band wavelet decomposition and comparisons with 2-band approaches, in: Proceedings of International Symposium on Intelligent Multimedia, Video and Speech Processing, Oct. 2004, pp. 623–626.
[41] C. Rao, G. Bhokare, U. Kumar, P. Patwardhan, V.M. Gadre, Tree structures and algorithms for hybrid transforms, in: International Conference on Signal Processing and Communications, July 2010, pp. 1–5.
[42] M. Kokare, B.N. Chatterji, P.K. Biswas, M-band wavelet based texture features for content based image retrieval, in: Indian Conference on Computer Vision, Graphics and Image Processing, 2002.
[43] S. Mallat, W.L. Hwang, Singularity detection and processing with wavelets, IEEE Trans. Inf. Theory 38 (2) (1992) 617–643.
[44] Z. Xu, A. Makur, On the arbitrary-length M-channel linear phase perfect reconstruction filter banks, IEEE Trans. Signal Process. 57 (10) (2009) 4118–4123.
[45] A. Papoulis, Signal Analysis, McGraw-Hill, New York, 1977.
[46] D. Slepian, Prolate spheroidal wave functions, Fourier analysis, and uncertainty–V: the discrete case, Bell Syst. Tech. J. 57 (5) (1978) 1371–1430.
[47] F.J. Simons, D.V. Wang, Spatiospectral concentration in the cartesian plane, GEM Int. J. Geomath. 2 (1) (2011) 1–36.
[48] Ç. Candan, M.A. Kutay, H.M. Ozaktas, The discrete fractional Fourier transform, IEEE Trans. Signal Process. 48 (5) (2000) 1329–1337.
[49] Y.V. Venkatesh, S.K. Raja, G. Vidyasagar, On the uncertainty inequality as applied to discrete signals, Int. J. Math. Math. Sci. 2006 (2006) 48185, 22 pp.
[50] J.D. Villasenor, B. Belzer, J. Liao, Wavelet filter evaluation for image compression, IEEE Trans. Image Process. 4 (8) (1995) 1053–1060.
[51] S. Oraintara, T.D. Tran, T.Q. Nguyen, A class of regular biorthogonal linear-phase filterbanks: theory, structure, and application in image coding, IEEE Trans. Signal Process. 51 (12) (2003) 3220–3235.
[52] J. Nocedal, S. Wright, Numerical Optimization, Springer Science & Business Media, 2006.
[53] M. Vetterli, C. Herley, Wavelets and filter banks: theory and design, IEEE Trans. Signal Process. 40 (9) (1992) 2207–2232.
[54] Y.-J. Chen, S. Oraintara, K.S. Amaratunga, Dyadic-based factorizations for regular paraunitary filterbanks and M-band orthogonal wavelets with structural vanishing moments, IEEE Trans. Signal Process. 53 (1) (2005) 193–207.
[55] L. Soares, H. De Oliveira, R. Cintra, R. de Souza, Fourier eigenfunctions, uncertainty Gabor principle and isoresolution wavelets, arXiv preprint arXiv:1502.03401, 2015.
[56] X. Mi, H. Ren, Z. Ouyang, W. Wei, K. Ma, The use of the Mexican hat and the Morlet wavelets for detection of ecological patterns, Plant Ecol. 179 (1) (2005) 1–19.
[57] R.G. Andrzejak, K. Lehnertz, F. Mormann, C. Rieke, P. David, C.E. Elger, Indications of nonlinear deterministic and finite-dimensional structures in time series of brain electrical activity: dependence on recording region and brain state, Phys. Rev. E 64 (6) (2001) 061907.
[58] R.B. Pachori, Discrimination between ictal and seizure-free EEG signals using empirical mode decomposition, Res. Lett. Signal Process. 2008 (2008) 293056.
[59] R. Kohavi, et al., A study of cross-validation and bootstrap for accuracy estimation and model selection, in: International Joint Conference on Artificial Intelligence, Stanford, CA, vol. 14, 1995, pp. 1137–1145.
[60] F.S. Bao, D.Y.-C. Lie, Y. Zhang, A new approach to automated epileptic diagnosis using EEG and probabilistic neural network, in: 20th IEEE International Conference on Tools with Artificial Intelligence, vol. 2, 2008, pp. 482–486.
[61] S. Altunay, Z. Telatar, O. Erogul, Epileptic EEG detection using the linear prediction error energy, Expert Syst. Appl. 37 (8) (2010) 5661–5665.
[62] V. Joshi, R.B. Pachori, A. Vijesh, Classification of ictal and seizure-free EEG signals using fractional linear prediction, Biomed. Signal Process. Control 9 (2014) 1–5.
[63] R.B. Pachori, S. Patidar, Epileptic seizure classification in EEG signals using second-order difference plot of intrinsic mode functions, Comput. Methods Programs Biomed. 113 (2) (2014) 494–502.
[64] R. Sharma, R.B. Pachori, Classification of epileptic seizures in EEG signals based on phase space representation of intrinsic mode functions, Expert Syst. Appl. 42 (3) (2015) 1106–1117.
[65] T.S. Kumar, V. Kanhangad, R.B. Pachori, Classification of seizure and seizure-free EEG signals using local binary patterns, Biomed. Signal Process. Control 15 (2015) 33–40.
[66] A.K. Tiwari, R.B. Pachori, V. Kanhangad, B.K. Panigrahi, Automated diagnosis of epilepsy using key-point-based local binary pattern of EEG signals, IEEE J. Biomed. Health Inform. 21 (4) (2017) 888–896.
[67] A. Bhattacharyya, R.B. Pachori, A. Upadhyay, U.R. Acharya, Tunable-Q wavelet transform based multiscale entropy measure for automated classification of epileptic EEG signals, Appl. Sci. 7 (4) (2017) 385.
[68] M. Sharma, R.B. Pachori, U.R. Acharya, A new approach to characterize epileptic seizures using analytic time–frequency flexible wavelet transform and fractal dimension, Pattern Recognit. Lett. 94 (July 2017) 172–179, http://www.sciencedirect.com/science/article/pii/S0167865517300995.

Dinesh Bhati received the B.E. degree in Electronics and Communication Engineering from Government Engineering College, Ujjain, India in 1999; the M.Sc. (Engg.) and Ph.D. degrees from Indian Institute of Science, Bangalore, India, in 2003 and Indian Institute of Technology Bombay, Mumbai, India, in 2017, respectively. His research interests include multirate filterbanks, wavelet transforms for 1-D and 2-D signal processing and their applications.

Ram Bilas Pachori received the B.E. degree with honors in Electronics and Communication Engineering from Rajiv Gandhi Technological University, Bhopal, India in 2001, the M.Tech. and Ph.D. degrees in Electrical Engineering from Indian Institute of Technology Kanpur, Kanpur, India in 2003 and 2008, respectively. He worked as a Postdoctoral Fellow at Charles Delaunay Institute, University of Technology of Troyes, Troyes, France during 2007–2008. He served as an Assistant Professor at Communication Research Center, International Institute of Information Technology, Hyderabad, India during 2008–2009. He served as an Assistant Professor at Discipline of Electrical Engineering, School of Engineering, Indian Institute of Technology Indore, Indore, India during 2009–2013, where presently he has been working as an Associate Professor since 2013. He worked as a Visiting Scholar at Intelligent Systems Research Center, Ulster University, Northern Ireland, UK during December 2014. His research interests are in the areas of biomedical signal processing, non-stationary signal processing, speech signal processing, signal processing for communications, computer-aided medical diagnosis, and signal processing applications.

Vikram M. Gadre received the B.Tech. and Ph.D. degrees in Electrical Engineering from the Indian Institute of Technology (IIT) Delhi, India, in 1989 and 1994, respectively. He is currently a Professor with the Department of Electrical Engineering, IIT Bombay, Mumbai, India. His research interests are broadly in the area of communication and signal processing, with emphasis on multi-resolution approaches. Dr. Gadre was the recipient of the President of India Gold Medal from IIT Delhi in 1989 and the Award for Excellence in Teaching from IIT Bombay in 1999, 2004, 2009 and 2014. He was also the recipient of the SVC Aiya Memorial Award and the Prof. K. Sreenivasan Medal from the Institution of Electronics and Telecommunication Engineers for contribution to education in Electronics and Telecommunication.